Laminar flame speeds of methanol and ethanol at high pressure and temperature conditions: An experimental and modeling approach

Bakr Hoblos, Guillaume Dayma, Fabien Halter, Zeynep Serinyel

Fuel 415 (2026) 138358

Contents lists available at ScienceDirect

Fuel

journal homepage: www.elsevier.com/locate/fuel

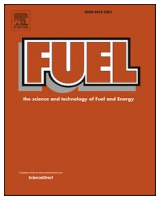

Full Length Article

Laminar flame speeds of methanol and ethanol at high pressure and temperature conditions: An experimental and modeling approach☆

Bakr Hoblos [a,b], Guillaume Dayma [a,b], Fabien Halter [a,b], Zeynep Serinyel [a,b,*]

[a] Université d'Orléans, 6 Avenue du Parc Floral, 45100 Orléans, France
[b] CNRS–ICARE, 1C Avenue de la Recherche Scientifique, 45071 Orléans cedex 2, France

ARTICLE INFO

Keywords:
Biofuel
Methanol
Ethanol
Laminar flame speed
Kinetic mechanism

ABSTRACT

During the last few decades, the importance of bio-derived components as efficient alternatives for fossil fuels has significantly increased; however, their full characterization has not been completed yet. Laminar flame speed is one of the fundamental properties characterizing a fuel and is used to validate chemical kinetic mechanisms. In the present study, laminar flame speeds were measured for various methanol/O_2 and ethanol/O_2 diluted mixtures over a large range of conditions, including equivalence ratios (0.7 to 1.4) and initial fresh gas temperatures (331 and 358 K) and pressures (0.5–4 bar). The experimental apparatus used to perform the flame speed measurements is the perfectly spherical combustion chamber with full optical access (OPTIPRIME) developed at ICARE laboratory. The flame propagation compressed the fresh gas, resulting in high pressure and temperature conditions, under which the flame speed increased up to 150 cm.s^{-1} for the tested methanol mixtures and 80 cm.s^{-1} for those of ethanol. Experimental uncertainties on flame speed were estimated to be within ± 5%. The extensive database obtained in this work was used to build flame speed correlations as functions of pressure and temperature, generating comprehensive maps for various equivalence ratios that can be refined with additional data to improve accuracy and extend the range of validity. A kinetic mechanism was also developed in this work and showed good performance in representing the present experimental data, taking into account their uncertainties. The mechanism was further validated against previously reported data (including species mole fractions and ignition delay times) on methanol and ethanol oxidation.

1. Introduction

Due to the high environmental impact of fossil fuels, their replacement in the near future will become inevitable and biofuels are among the most important possible alternatives. However, before they could be used in combustion systems, biofuels still need in-depth knowledge especially in terms of their oxidation kinetics. Their reaction mechanisms should be tested and validated over a wide range of physical conditions (such as pressure, temperature, and equivalence ratio), in different experimental regimes, and for various types of data (e.g., ignition delay times, species mole fractions, etc.) to accurately capture their chemical behavior under realistic combustion conditions. In this context, the laminar burning velocity, sometimes referred to as the laminar flame speed, is a key fundamental combustion property to be studied in the widest possible operating conditions. The data on such a property are very important for the validation of kinetic models, especially in an attempt to have a robust core mechanism. The present study involves two common fuels that can be produced from biomass and which substantially contribute to the base mechanism of kinetic models, methanol and ethanol. In accordance with the foregoing, the laminar flame speeds of these two simple alcohols have been widely measured in previous works and under different conditions. A table was added in the supplementary material (Table S1) to show the main set of these studies.

Most studies on laminar burning velocity measurements were experimentally restricted to narrow ranges and non-simultaneous variations of pressure and temperature. However, this limitation has been overcome by using spherically expanding flames with the isochoric method [1,2]. This constant-volume technique is incredibly more performant than the isobaric method, since it provides a trace of flame speed for each combustion as the flame propagates; i.e., as pressure and

☆ This article is part of a special issue entitled: 'MCS13' published in Fuel.

* Corresponding author at: CNRS–ICARE, Institut de Combustion, Aérothermique, Réactivité et Environnement , 1C Avenue de la Recherche Scientifique, 45071 Orléans cedex 2, France.
E-mail address: zeynep.serinyel@cnrs-orleans.fr (Z. Serinyel).

https://doi.org/10.1016/j.fuel.2026.138358
Received 21 October 2025; Received in revised form 23 December 2025; Accepted 11 January 2026
Available online 22 January 2026

temperature increase simultaneously in an isentropic manner. Konnov et al. [3] published a detailed comprehensive review investigating laminar burning velocities for various mixtures of air and fuels, including methanol and ethanol. The examination of this bibliographic study reveals clear discrepancies and gaps in the laminar burning velocity data persisting even for such basic fuels, particularly at elevated temperatures and pressures, as well as inconsistencies in the performance of the most recent kinetic mechanisms in predicting these data. This indicates that research in this field has not yet come to an end and highlights the need for further investigations and the continued development of kinetic mechanisms. Nevertheless, it is useful first to go through some of the important works previously published in the domain, which highlight the relevance of the present study (more established studies could be found in Table S1, as mentioned before). Gülder [4] used an isochoric spherical bomb to measure the laminar flame speeds of methanol/air and ethanol/air mixtures. His experimental work covered equivalence ratios from 0.7 to 1.4, an initial pressure range of 1–8 bar, and an unburnt gas temperature range of 300–500 K. Veloo et al. [5] measured the flame speeds of methanol/air and ethanol/air mixtures in the counterflow configuration at atmospheric pressure, a fresh gas temperature of 343 K, and an equivalence ratio range (0.7–1.5). Beeckmann et al. [6] reported laminar burning velocities of spherically expanding flames of methanol and ethanol mixtures in air at 10 bar, 373 K, and equivalence ratios ranging from 0.7 to 1.33. They also evaluated existing kinetic mechanisms against their data. While these models performed reasonably well at atmospheric pressure, they underpredicted the experimental results at 10 bar. Based on sensitivity analysis, the authors concluded that the base mechanisms must be refined using high-pressure burning velocity data for both alcohols. Raida et al. [7] used a heat flux burner setup to measure the burning velocities of methanol/air and ethanol/air flames up to a pressure of 5 bar, for inlet temperatures of 318–338 K, and at equivalence ratios going from 0.8 to 1.3. Similar to the previous study, they found good agreement between literature mechanisms and atmospheric-pressure data, but systematic scatter at high pressures, both between models and experiments as well as among the data themselves. Thus, they confirmed the need for further studies to expand the pressure range of available data for the development and refinement of kinetic models. More recently, Zheng et al. [8] evaluated the flame speeds of methanol/O_2/Ar using the shock tube method at pressures up to 2.6 bar, high temperatures ranging from 640 to 916 K, and equivalence ratios up to 1.4. Furthermore, this team published a similar work for ethanol at elevated temperatures, where they additionally conducted atmospheric-pressure experiments for stoichiometric ethanol/air mixtures between 453 and 524 K [9]. In both studies, the authors observed model discrepancies and suggested possible adjustments to the rate constants of key sensitive reactions, including fuel-specific and small-molecule reactions, aiming to reduce the disagreement between models and data.

The present study aims to provide novel laminar flame speed data for methanol and ethanol over a wide range of conditions, including scarcely explored high pressures and high temperatures. Given that commonly used kinetic mechanisms in the literature fail to reproduce the present experimental data, this work also aims to develop a more robust core mechanism, demonstrating improved predictive capability while showing good agreement with other datasets previously reported for both investigated fuels.

2. Experimental setup

All experiments were carried out in OPTIPRIME, the perfectly spherical combustion chamber with full optical access developed at ICARE laboratory [10,11]. This isochoric chamber is equipped with a 360° fused silica ring allowing a full radial visualization of the flame propagation from the central ignition to the wall. The ring was designed with an internal diameter identical to that of the chamber to ensure a perfectly spherical propagation for the flame without any surface deformation. Two sensors (AVL GU21D) – diametrically opposed in the chamber – are used to monitor the pressure, while a K-type thermocouple is used to control the initial unburnt gas temperature. The combustion chamber is located in a furnace in order to perform homogeneous heating. An illustration of the experimental apparatus can be found in the supplementary material (Fig. S1).

Table 1
Initial mixture conditions tested and resulting ranges of pressure and temperature of the fresh gas.

Fuel	Oxidizer-Diluent	T_0 (K)	p_0 (bar)	Equivalence ratio	T (K)	p (bar)
CH_3OH	O_2-N_2 (Air)	358	0.5, 1, 2	0.7, 0.8, 0.9, 1, 1.1	429–569	1.1–9.1
CH_3OH	O_2-N_2 (Air)	358	0.5, 1	1.2, 1.3, 1.4	432–564	1.2–5.8
CH_3OH	O_2-He/Ar	358	4	0.85, 1, 1.2, 1.36	469–612	9.2–21.3
C_2H_5OH	O_2-N_2 (Air)	331	1, 2, 3	0.7	390–501	2.1–14.2
C_2H_5OH	O_2-N_2 (Air)	331	1, 2	1	390–517	2.0–6.3
C_2H_5OH	O_2-N_2 (Air)	331	0.5, 1	1.2	390–530	1.1–5.0

Initially in liquid phase, both fuels were injected using a syringe, where they were quickly evaporated and directed to the chamber. The other gases, oxidizer (O_2) and diluent (N_2 or He/Ar), were then successively introduced using the partial pressure method. The experiments were subsequently conducted and both pressure (p) and flame radius (R_f) evolutions were simultaneously recorded to calculate the corresponding laminar flame speeds (S_u) with the isochoric method using the following differential equation:

$$S_u = \frac{dR_f}{dt} - \frac{\left({R_0}^3 - {R_f}^3\right)}{3\gamma_u {R_f}^2} \times \frac{dp}{dt} \quad (1)$$

where R_0 is the internal chamber radius, γ_u is the heat capacity ratio of the unburnt gas, and t is the time. A precision less than 0.5% on the radius determination led to an uncertainty on the flame speed measurement that can be estimated to be within ± 5%. This uncertainty has been taken into account by thickening the experimental traces shown in the results section. These traces are usually plotted within a relative range of pressure with respect to its initial value: $2 < p/p_0 < 5$, to avoid both stretch effect and heat loss to the wall. The detailed experimental setup and methodology used to evaluate the flame speed evolution, along with the associated uncertainty, are described in [10,11].

Various conditions of initial pressures ($p_0 = 0.5$, 1, 2, and 4 bar) and temperatures ($T_0 = 331$ and 358 K) were studied. Different equivalence ratios (φ) were also selected: fuel-lean mixtures ($\varphi = 0.7$, 0.8, and 0.85), stoichiometric/near-stoichiometric conditions ($\varphi = 0.9$, 1, and 1.1), and fuel-rich mixtures (φ = 1.2, 1.3, 1.36, and 1.4). The oxidizer/diluent mixture used was either air (O_2/N_2: 21/79) or O_2/Ar/He blend (15/17/68). In fact, from a stability point of view, the dilution with N_2 was not feasible under certain conditions, particularly at high initial pressures, where the use of a He/Ar mixture was more relevant to guarantee flame propagation without instabilities [12]. The studied conditions are listed in Table 1, and the experimental data obtained are provided as supplementary material.

3. Kinetic modeling

All simulations, including those of literature data, were carried out using the software ANSYS Chemkin 2024 R2 [13]. The flame speed simulations were done using the premixed laminar flame speed calculation model with thermal diffusion, applying strict solution conditions with GRAD and CURV values of 0.02, resulting in a maximum of 3000 grid points. For the speciation data and ignition delay times obtained in

Table 2
Tested chemical kinetic mechanisms.

Mechanisms	#Species	#Reactions*	Fuels tested
Present work	56	471	CH_3OH, C_2H_5OH
Mech15.34 [15]	173	1011	CH_3OH
HPMech [16]	131	899	CH_3OH
Mittal et al. [17]	68	390	C_2H_5OH
Millán-Merino et al. [18]	34	69	C_2H_5OH
POLIMI C_1-C_3 [19]	114	1999	CH_3OH, C_2H_5OH
AramcoMech3.0 [20]	581	3037	CH_3OH, C_2H_5OH

* Duplicate reactions were counted individually.

jet-stirred reactors (JSRs) and shock tubes, the simulations were performed using the perfectly stirred reactor and the closed homogeneous batch reactor models, respectively. A new kinetic mechanism is proposed for methanol and ethanol in the current work, based on the C_0–C_2 core mechanism of our recently published study [14]. It is provided in the supplementary material, along with the corresponding thermochemical and transport data, and will also be available on our website (https://www.univ-orleans.fr/fr/groupe-combustion/oxygenates) after publication. Simulations were also done using kinetic mechanisms from the literature in order to test their performance on the present experimental data. These mechanisms are listed in Table 2, specifying the number of species and reactions for each, and whether they have been tested against the present data of methanol and/or ethanol. The mechanism of Burke et al. [15], Mech15.34, was validated against various methanol data determined under engine relevant conditions, while that of Wang et al. [16], HPMech, was designed particularly for supercritical-pressure methanol oxidation. Mittal et al. [17] mechanism was proposed primarily for ethanol autoignition in a rapid compression machine, while that of Millán-Merino et al. [18] is a skeletal model suggested and validated for both premixed flame propagation and autoignition of ethanol. Finally, POLIMI C_1-C_3 [19] and AramcoMech3.0 [20] are multi-purpose mechanisms validated on different targets and for various fuels, including methanol and ethanol.

4. Results

For the different mixtures studied in this work, the laminar flame speed (S_u) was plotted as a function of the pressure (p) and temperature (T): an axis (for each p_0) was added at the top of each graph to show the isentropic increase of T with p due to the compression of the fresh gases induced by the flame front propagation. The transparency of the gray experimental traces and T-axes was decreased as p_0 increases to better

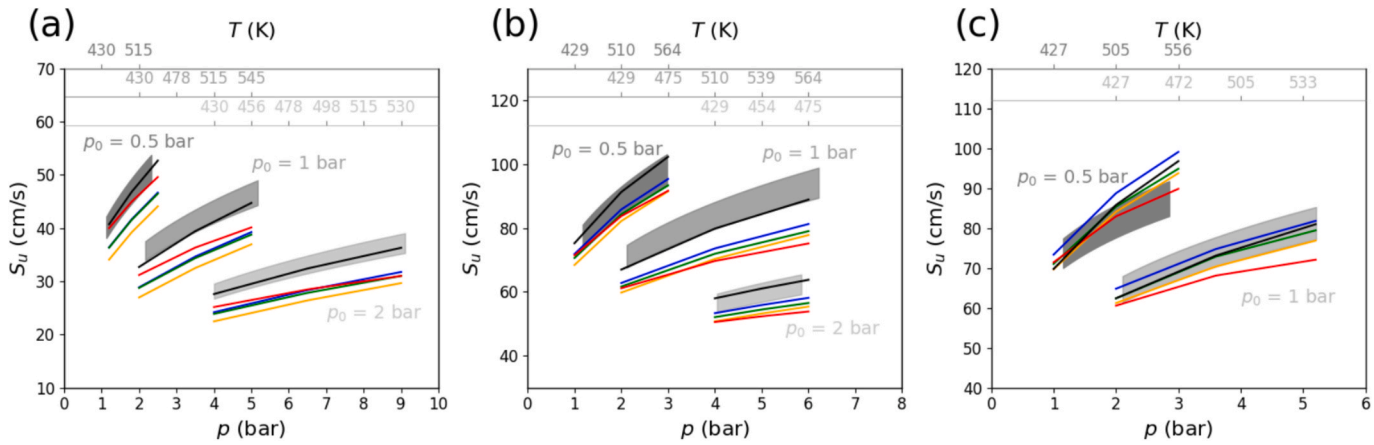

Fig. 1. Methanol/air flame speed evolution as a function of pressure and temperature for $\varphi = 0.7$ (a), 1 (b), and 1.4 (c). These mixtures were tested under the same initial temperature $T_0 = 358$ K. Thickened gray traces correspond to experimental results with their associated uncertainty (± 5%). Lines correspond to simulations: Black: present work – Green: Mech15.34 [15] – Red: HPMech [16] – Blue: POLIMI C_1-C_3 [19] – Orange: AramcoMech3.0 [20]. (For interpretation of the references to colour in this figure legend, the reader is referred to the web version of this article.)

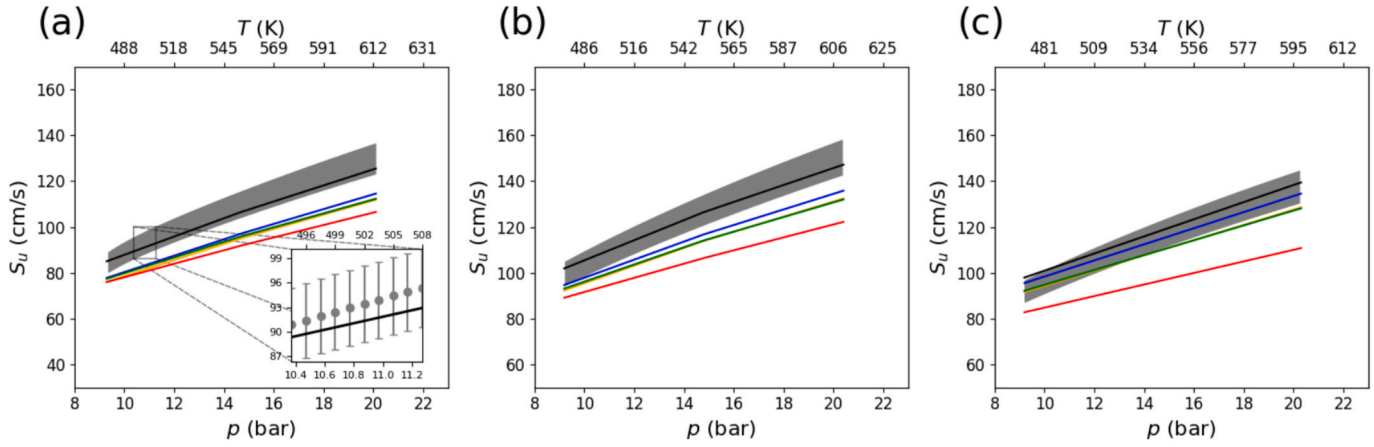

Fig. 2. Methanol/O_2/He/Ar flame speed evolution as a function of pressure and temperature for $\varphi = 0.85$ (a), 1 (b), and 1.36 (c). These mixtures were tested under the same initial pressure ($p_0 = 4$ bar) and temperature ($T_0 = 358$ K). Thickened gray traces correspond to experimental results with their associated uncertainty (± 5%). Lines correspond to simulations: Black: present work – Green: Mech15.34 [15] – Red: HPMech [16] – Blue: POLIMI C_1-C_3 [19] – Orange: AramcoMech3.0 [20]. (For interpretation of the references to colour in this figure legend, the reader is referred to the web version of this article.)

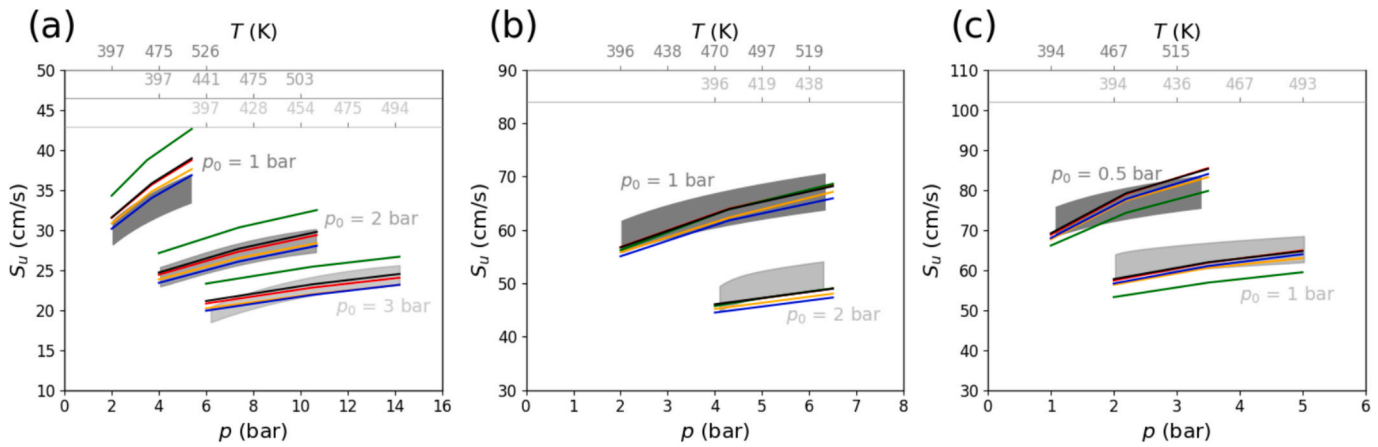

Fig. 3. Ethanol/air flame speed evolution as a function of pressure and temperature for $\varphi = 0.7$ (a), 1 (b), and 1.2 (c). These mixtures were tested under the same initial temperature $T_0 = 331$ K. Thickened gray traces correspond to experimental results with their associated uncertainty (± 5%). Lines correspond to simulations: Black: this work – Red: Mittal et al. [17] – Green: Millán-Merino et al. [18] – Blue: POLIMI C_1-C_3 [19] – Orange: AramcoMech3.0 [20]. (For interpretation of the references to colour in this figure legend, the reader is referred to the web version of this article.)

distinguish between its distinct values in the same graph. The main resulting plots are presented in the following sub-sections (Figs. 1–3), while the remaining plots for similar conditions are provided in the supplementary material (Fig. S2), along with a 3D representation of $S_u = f(p,\varphi)$ at $p_0 = 1$ bar (Fig. S3). In order to clarify the representation of experimental traces, a zoomed-in section was included in Fig. 2a as an illustrative example.

4.1. Methanol mixtures

Fig. 1 shows the experimental and simulated plots $S_u = f(p,T)$ obtained for the methanol/air mixtures tested at $\varphi = 0.7$, 1, and 1.4. Under both lean and stoichiometric conditions, the present mechanism gives the best prediction for our experimental data compared to the other models tested; the S_u simulated by our mechanism stays within the corresponding uncertainty range (or at the lowest limit of this range in the worst case). On the other hand, it can be seen that the literature mechanisms underpredict the experimental results for both lean and stoichiometric mixtures, although they (all except HPMech) show better predictions for the latter compared to the former. When the mixture becomes rich, there is good agreement between the experimental and computed S_u at $p_0 = 1$ bar with all mechanisms except HPMech. As for the lean and stoichiometric mixtures, the latter continues to underestimate the experimental data. However, at $p_0 = 0.5$ bar, it provides the best prediction, while the simulations from the other mechanisms initially match the experimental trace but then tend to slightly overestimate S_u above a certain value of pressure and temperature (varying from a mechanism to another), with POLIMI C_1-C_3 showing the highest overprediction.

Flame speeds of the methanol/O_2 mixtures, diluted in the He/Ar blend and tested at a high initial pressure $p_0 = 4$ bar, are presented in Fig. 2, as functions of the pressure. The present mechanism predicts very well these experimental data for all equivalence ratios tested, while the literature mechanisms underpredict them, as they did with the previous data. This underprediction becomes less pronounced with the increase of the equivalence ratio for Mech15.34, AramcoMech3.0 (coinciding with the latter), and POLIMI C_1-C_3 (which is inside the uncertainty range at the rich condition).

4.2. Ethanol mixtures

Fig. 3 exhibits the experimental and computed plots $S_u = f(p,T)$ obtained for the ethanol/air mixtures studied at $\varphi = 0.7$, 1, and 1.2. The present model and that of Mittal show very close simulations for all these mixtures.

For the fuel-lean mixture, S_u is overpredicted highly by the model of Millán-Merino and slightly by the present model and that of Mittal when $p_0 = 1$ bar, while AramcoMech3.0 and POLIMI C_1-C_3 are showing simulations near or at the upper limit of the experimental trace. Then, the discrepancies between the experimental results and the simulations decrease when p_0 increases to 2 and 3 bar. Thus, S_u becomes better predicted for these two initial pressures by all the mechanisms except for the skeletal mechanism of Millán-Merino, which continues to overestimate the experimental trace.

At the stoichiometric condition, all the simulations are in good agreement with the experimental data when $p_0 = 1$ bar, with our mechanism and those of Mittal and Millán-Merino showing the best estimation. When p_0 increases to 2 bar, the simulations underpredict the experimental data: all S_u computed remain at the lowest edge of the experimental trace, with POLIMI C_1-C_3 and AramcoMech3.0 showing the less accurate estimations remaining below the uncertainty range.

For the rich mixture, the mechanisms show generally good predictions at $p_0 = 0.5$ bar, even though the present one and that of Mittal display a slight overprediction, similar to what was seen for methanol under a similar condition. Only the skeletal mechanism shows an underestimation for the experimental trace when $p < 2$ bar, but then provides a better prediction within this trace at higher pressures. When p_0 increases to 1 bar, all tested mechanisms predict reasonably well the present data, except for the skeletal model, which shows a relatively significant underestimation.

Finally, it is worth noting that, although the skeletal mechanism shows good agreement for stoichiometric mixtures, it exhibits large discrepancies at lean and rich conditions relative to experimental data and detailed mechanisms, highlighting its insufficiency in predicting flame speeds over a wide range of conditions.

5. Sensitivity analyses

In this section, sensitivity analyses are performed on the flow rate in order to identify the key reactions controlling the flame speed evolution for both methanol and ethanol. The analyses were carried out using the present mechanism since it showed the best prediction for the current experimental data. For each condition, the most sensitive reactions identified could be classified in two different groups based on their effect on the flame speed: those promoting S_u (having a sensitivity coefficient $S > 0$) and those inhibiting S_u (with $S < 0$). For each fuel, two equivalence ratios were considered with three different pressures and their corresponding temperatures. Similar to the results presented in the previous

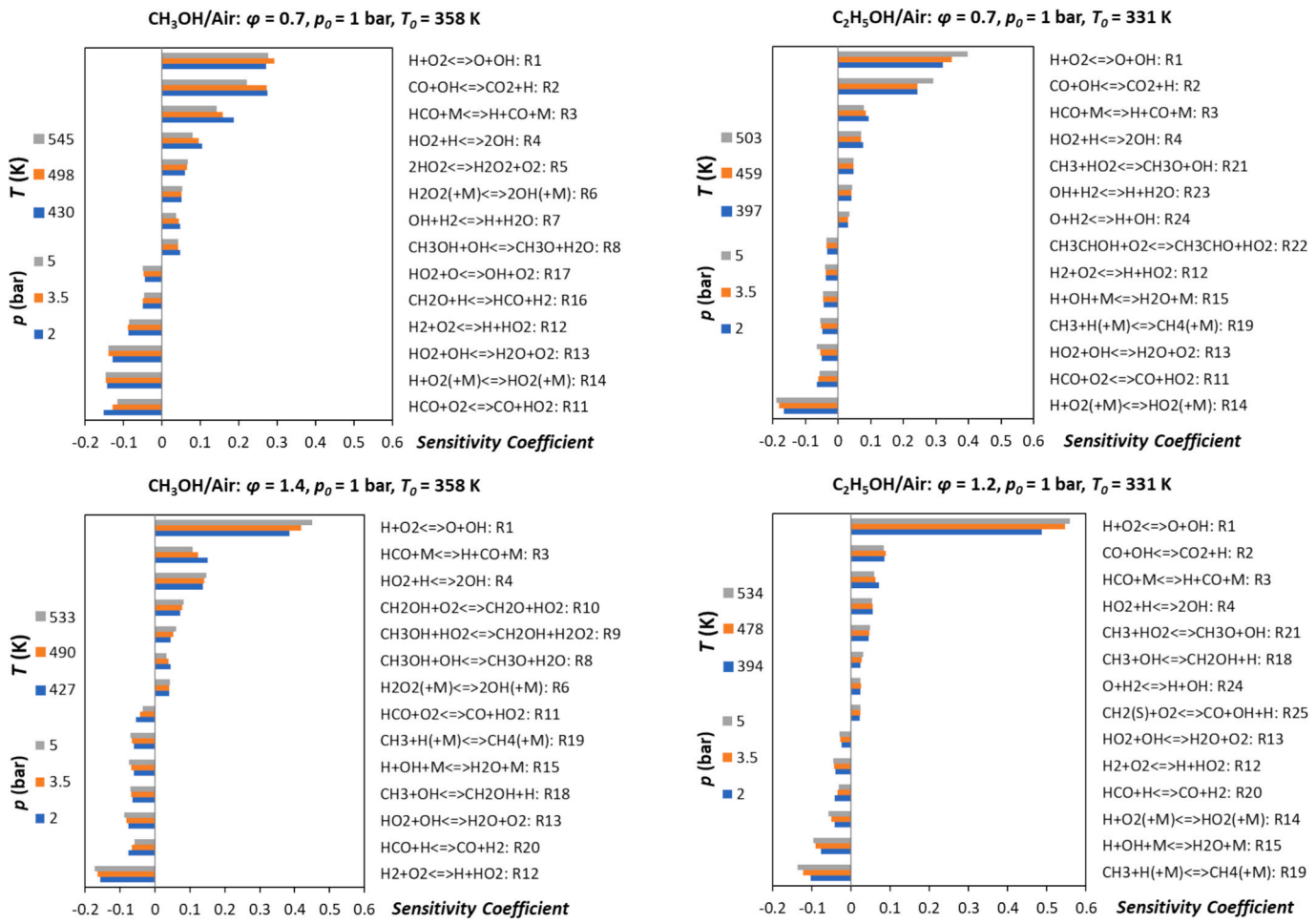

Fig. 4. Sensitivity analyses performed on the flow rate using the present mechanism at two different equivalence ratios for: methanol/air (left) and ethanol/air (right) mixtures.

section, sensitivities at a given φ are described in terms of pressure only, as the associated temperature variation follows the same trend.

5.1. Methanol mixtures

Fig. 4 (left) illustrates the sensitivity analyses done for methanol/air mixtures at $\varphi = 0.7$ and 1.4. As far as promoting reactions are concerned, in any condition, and as expected, $H + O_2 \rightleftharpoons O + OH$ (R1) is the most positively sensitive reaction and its sensitivity significantly increases with φ. In the second place, appears the reaction $CO + OH \rightleftharpoons CO_2 + H$ (R2), which is highly sensitive at the lean condition but less sensitive as φ increases, and not sensitive when the mixture is rich. Although it consumes the highly reactive OH radicals, this reaction supplies H atoms to the chain-branching reaction R1. $HCO + M \rightleftharpoons H + CO + M$ (R3) comes thirdly in the promoting group, providing H to R1 and CO to R2, and shows decreasing sensitivity with increasing φ or p. Although it consumes H atoms, $HO_2 + H \rightleftharpoons 2OH$ (R4) has a positive sensitivity coefficient, as each H consumed generates two OH radicals. This coefficient increases with an increase in equivalence ratio, as the H atoms become more abundant at rich conditions. In addition, the two reactions $2HO_2 \rightleftharpoons H_2O_2 + O_2$ (R5) and $H_2O_2 (+M) \rightleftharpoons 2OH (+M)$ (R6) appear among the promoting reactions with a sensitivity that decreases with the equivalence ratio, since HO_2 radicals and subsequently H_2O_2 molecules (produced from the HO_2 self-disproportionation) become less abundant. Moreover, $OH + H_2 \rightleftharpoons H + H_2O$ (R7) and $CH_3OH + OH \rightleftharpoons CH_3O + H_2O$ (R8) promote the reactivity but become less sensitive when increasing φ or p. Furthermore, two fuel-specific reactions appear in the promoting list at the rich condition: $CH_3OH + HO_2 \rightleftharpoons CH_2OH + H_2O_2$ (R9) and $CH_2OH + O_2 \rightleftharpoons CH_2O + HO_2$ (R10), which have an increasing sensitivity with the pressure rise.

On the other hand, $HCO + O_2 \rightleftharpoons CO + HO_2$ (R11), which competes with HCO dissociation (R3), is the most important negatively sensitive reaction (inhibiting overall reactivity) at lean conditions (given the abundance of O_2). However, as φ increases, the sensitivity of this reaction decreases while that of $H_2 + O_2 \rightleftharpoons H + HO_2$ (R12) increases. Thus, the latter reaction (occurring in the reverse direction as a terminating step) becomes the most inhibiting reaction at the rich condition for all pressures. In addition, the sensitivity of R11 also decreases as the pressure increases to be exceeded by those of the terminating reaction $HO_2 + OH \rightleftharpoons H_2O + O_2$ (R13) and the recombination $H + O_2 (+M) \rightleftharpoons HO_2 (+M)$ (R14) (converting H into the less reactive HO_2) for $p > 2$ bar. The latter becomes less sensitive with the increase of φ (as O_2 concentration decreases) and disappears from the list at the rich condition, while a new recombination reaction appears: $H + OH + M \rightleftharpoons H_2O + M$ (R15), whose sensitivity coefficient increases with pressure. $CH_2O + H \rightleftharpoons HCO + H_2$ (R16) (becoming less sensitive when p increases) and $HO_2 + O \rightleftharpoons OH + O_2$ (R17) (becoming more sensitive when p increases) have an inhibiting effect on the reactivity as well. These two reactions disappear from the list when the mixture is rich, while two new inhibiting reactions appear (given the abundance of CH_3 radicals at rich conditions): $CH_3 + OH \rightleftharpoons CH_2OH + H$ (R18) and $CH_3 + H (+M) \rightleftharpoons CH_4 (+M)$ (R19), the latter consuming H atoms to form stable methane molecules. Finally, the reaction $HCO + H \rightleftharpoons CO + H_2$ (R20) appears in the inhibiting group (as it both competes with R3 and consumes H) at the rich condition (due to the

abundance of H atoms), with a sensitivity that decreases when the pressure increases.

We can conclude that, despite the dominance of the reactions of syngas submechanism on the list of the most sensitive reactions, the fuel-related reactions (R8–10 and R18) still have their impact on the flame speed, especially under rich conditions. These four reactions are: the H-abstraction of methanol by OH (forming CH_3O) and by HO_2 (forming CH_2OH), as well as the subsequent reactions of the latter with O_2 (producing formaldehyde and HO_2) and with H (producing CH_3 and OH). In addition, these sensitivity analyses provide insight into the discrepancies between previous mechanisms and the present one, which can explain their respective predictive performances and help future improvements. For instance, the underestimation of most present data by HPMech can be mainly attributed to a rate constant of R3 that is an order of magnitude lower than that used in the present mechanism. In contrast, the highest flame speeds predicted by POLIMI C_1-C_3 at $\varphi = 1.4$ arise from an $\approx 10\%$ increase in the pre-exponential factor of R1 relative to the present and other mechanisms: this small increase can have a significant effect on flame speed, especially under rich conditions, as the sensitivity of R1 strongly increases with equivalence ratio.

5.2. Ethanol mixtures

Fig. 4 (right) exhibits the sensitivity analyses done for ethanol/air mixtures at $\varphi = 0.7$ and 1.2. The most sensitive reactions in this case are almost the same as for methanol, excluding those that were specific for the latter. However, additional reactions can be identified in the case of ethanol, such as: $CH_3 + HO_2 \rightleftharpoons CH_3O + OH$ (R21) which promotes reactivity by converting the less reactive HO_2 into OH, and $CH_3CHOH + O_2 \rightleftharpoons CH_3CHO + HO_2$ (R22) which inhibits reactivity by diverting the fuel radical away from direct production of reactive radicals. In fact, while the favored radical of methanol, CH_2OH, leads mainly to formaldehyde and subsequently to HCO chemistry, the dominant radical of ethanol, CH_3CHOH, produces primarily acetaldehyde, which in turn forms acyl radicals that undergo α-scission to yield CH_3 radicals. This difference explains the higher sensitivity of HCO reactions for methanol and, in contrast, the higher sensitivity of CH_3 reactions for ethanol. Finally, it is worth noting that R18 shows opposite sensitivity for ethanol when compared to methanol. It is negatively sensitive for methanol, as it proceeds in the reverse direction due to the abundance of its primary radicals CH_2OH, thus competing with R1 for H atoms. In contrast, it is positively sensitive for ethanol, as it occurs in the forward direction (due to CH_3 abundance), thereby producing H atoms for R1.

Therefore, apart from syngas chemistry, the evolution of ethanol flame speed depends mainly on methane submechanism; only one reaction related to the fuel subset appears in the list of most sensitive reactions: R22, the reaction of ethanol secondary radical (CH_3CHOH) with O_2 forming acetaldehyde and HO_2, seen only at the lean condition (where O_2 is more concentrated) and as the lowest negatively sensitive reaction.

Overall, the sensitivity analyses show that, while the sensitivities of most reactions for both fuels exhibit large variations with equivalence ratio, they change only slightly with pressure and temperature at a fixed φ, consistent with how the flame speed of each fuel varies with these parameters (see Fig. S3 for a clearer comparison of the respective impacts of p and φ on S_u). The effects of pressure and temperature rise during flame propagation manifest primarily through R1 ($H + O_2 \rightleftharpoons O + OH$), the most sensitive reaction under all conditions. The sensitivity of the reaction R2 ($CO + OH \rightleftharpoons CO_2 + H$) becomes comparable to that of R1 only under lean conditions. The increase in the rate constant of R1 with temperature is the main driver of the rise in flame speed during propagation, whereas the flame speed evolution with equivalence ratio arises from broader reaction-pathway shifts rather than a limited set of reactions.

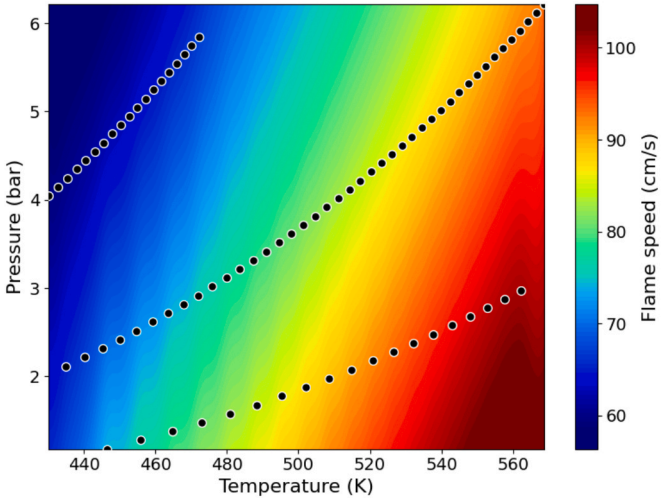

Fig. 5. Correlation map of methanol/air laminar flame speed as a function of pressure and temperature at $\varphi = 1$ (black circles represent the experimental data).

6. Correlation

Using the OPTIPRIME setup, each firing captures flame speeds over a large range of (p,T) conditions. By varying initial pressures across multiple firings, a dataset covering a wider domain can be generated and used to construct a correlation $S_u = f(p,T)$, enabling interpolation and extrapolation to map flame speeds efficiently. This approach can establish a versatile database of flame speeds for different mixtures and conditions, supporting CFD combustion modeling with minimal experiments.

The $S_u = f(p,T)$ correlation used here for methanol, previously applied to methane [21], is based on the initial flame speed $S_{u,i}$ at reference conditions p_i and T_i, as expressed in Eq. (2). The laminar burning velocity depends on temperature and pressure through two empirical exponents, α_T and β_P, which together include five tunable coefficients to fit the experimental traces.

$$S_u = S_{u,i} \times (T/T_i)^{\alpha_T} \times (p/p_i)^{\beta_p} \quad (2)$$

The correlation parameters are listed in the supplementary material. Each equivalence ratio has its own set of parameters, resulting in multiple flame speed maps. Fig. 5 presents the stoichiometric methanol/air case, with experimental results shown as black points and the remaining regions interpolated or extrapolated across the tested pressure and temperature range. These maps provide a practical way to estimate flame speed variation with pressure and temperature, with accuracy improving as additional data are incorporated. The extrapolation of these correlations to existing literature data is discussed in the supplementary material.

7. Further validation

In order to verify its performance, the present mechanism was tested on different literature data of methanol and ethanol in this section and showed a good prediction for them. More validation plots are also available in the supplementary material.

Fig. 6 shows the good performance of the present mechanism in predicting the evolution of laminar flame speed with pressure for methanol and ethanol reported by Raida et al. [7], although it slightly overestimated them for the near-stoichiometric mixture ($\varphi = 1.1$). Furthermore, this mechanism represents reasonably well the evolution of flame speed for both fuels with equivalence ratio and temperature (see Figs. S5–8).

Figs. 7 and 8 show the experimental and simulated mole fraction

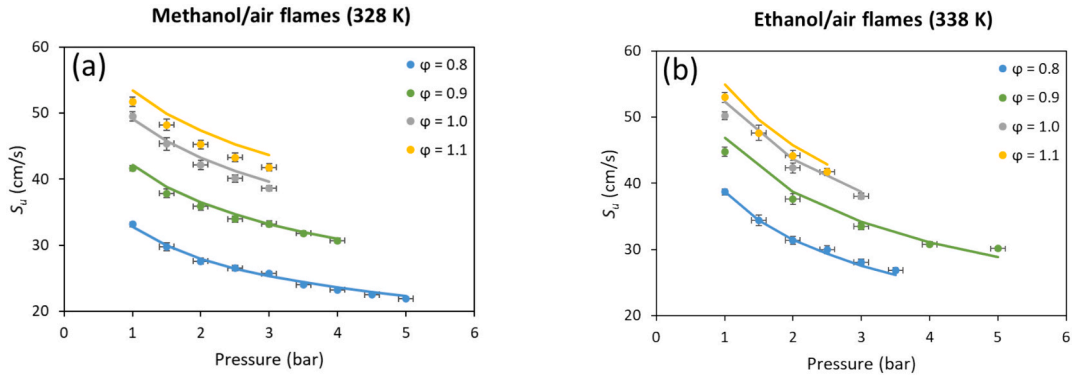

Fig. 6. Laminar burning velocities as functions of pressure for (a) methanol/air flames at 328 K and (b) ethanol/air flames at 338 K. Symbols: experiments (Raida et al. [7]); lines: simulations (present mechanism).

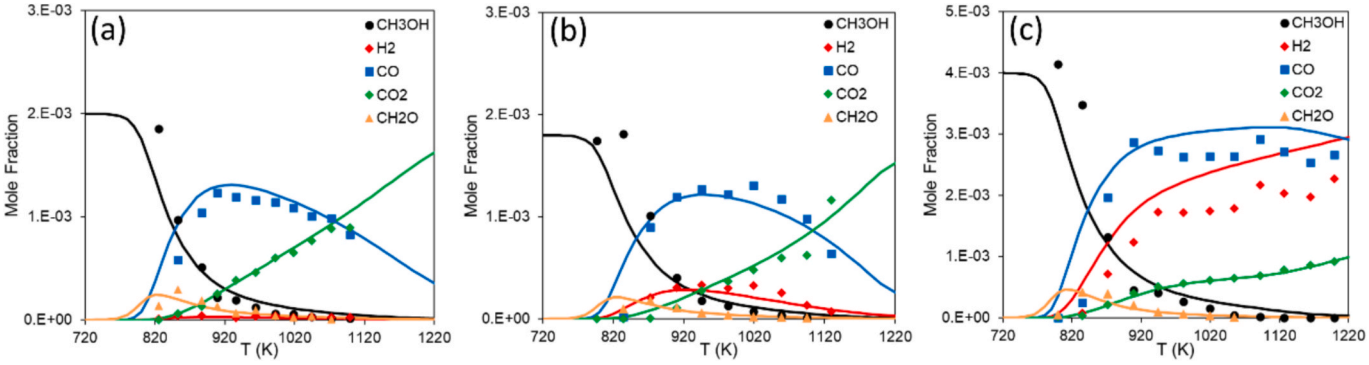

Fig. 7. Experimental (symbols: Burke et al. [15]) and computed (lines: this work) mole fraction profiles of species obtained during methanol oxidation in a JSR at p = 10 atm, τ = 0.5 s, and φ = 0.2 (a) / 1 (b) / 2 (c).

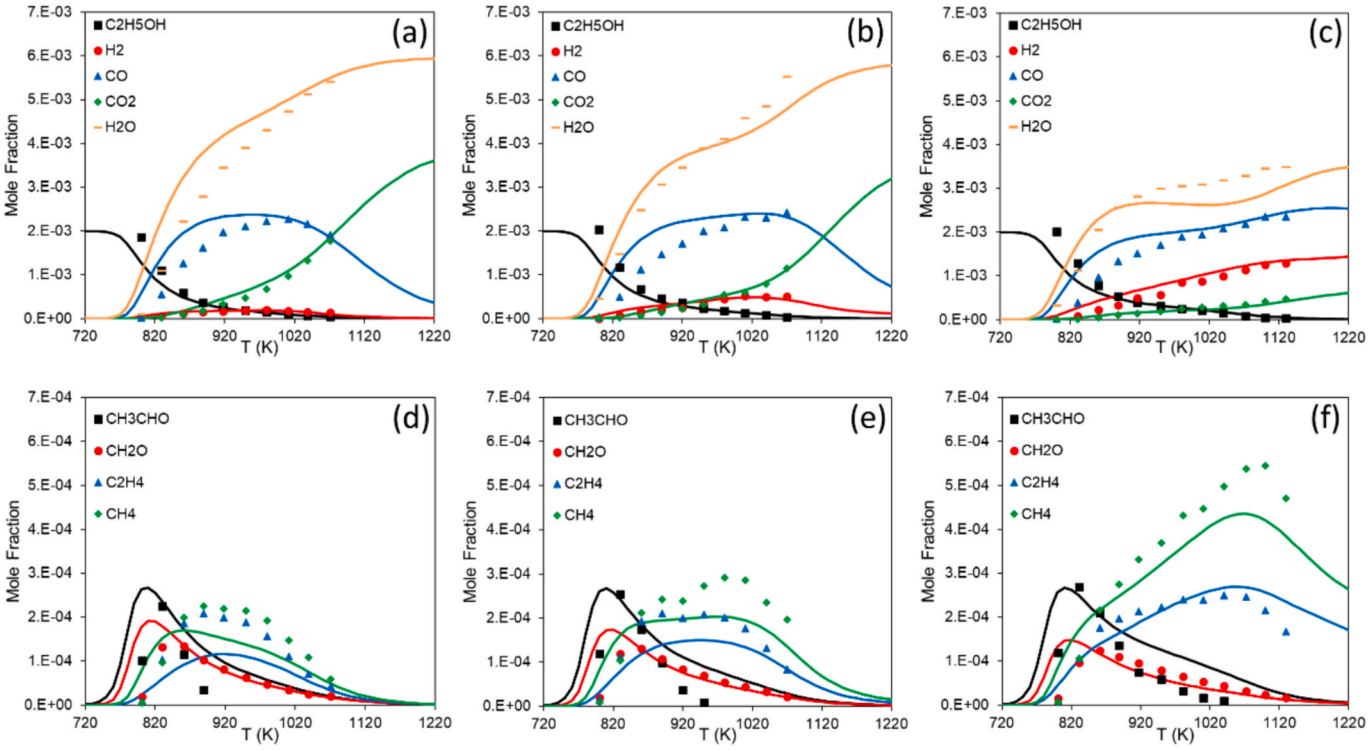

Fig. 8. Experimental (symbols: Leplat et al. [22]) and computed (lines: this work) mole fraction profiles of species obtained during ethanol oxidation in a JSR at p = 10 atm, τ = 0.7 s, and φ = 0.6 (a,d) / 1 (b,e) / 2 (c,f).

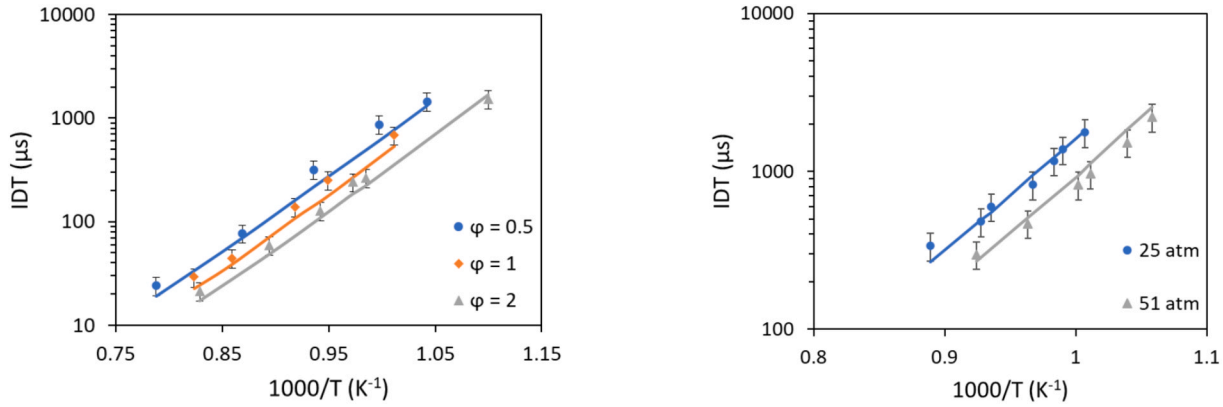

Fig. 9. Experimental (symbols) ignition delay times of different methanol/air mixtures measured by Burke et al. [15] at 50 atm (left) and of stoichiometric ethanol/air mixtures measured by Mathieu et al. [23] at about 25 and 50 atm (right) in shock tubes, with simulations using the present mechanism (lines).

profiles of species obtained at 10 atm with comparable residence times (τ), under three different equivalence ratios, from JSR oxidation of methanol [15] and ethanol [22], respectively. It can be noted that, although the present mechanism underpredicts the mole fractions of both fuels under 900 K, it becomes in better agreement with them at higher temperatures. The mechanism also successfully reproduces the general tendency of mole fraction variation with temperature for the different species formed during the oxidation of methanol and ethanol, including formaldehyde and acetaldehyde. Moreover, it captures well the influence of the equivalence ratio on the species profiles, which – for the fuels and aldehydes – appears to be limited to slightly shifting their complete consumption toward higher temperatures. It additionally enhances the formation of hydrogen and hydrocarbons and delays their conversion and that of CO into H_2O and CO_2, as expected from the reduced oxygen concentration associated with increasing equivalence ratio. Additional speciation data were also validated with the present mechanism for both fuels in the supplementary material (Figs. S12–S14).

Finally, Fig. 9 (along with Figs. S10 and S11) shows that the present mechanism successfully captures the observed decrease in ignition delay time with increasing pressure and/or equivalence ratio, and accurately reproduces the measured values for both methanol [15] and ethanol [23].

8. Conclusion

The laminar flame speeds of methanol/O_2 and ethanol/O_2 diluted mixtures were measured under fuel-lean, stoichiometric, and fuel-rich conditions. Two different diluents were used: either N_2 or He/Ar blend. Various initial pressures (up to 4 bar) and temperatures (331 and 358 K) were also selected, allowing flame speed measurements at pressures that can exceed 20 bar. All the experiments were carried out in OPTIPRIME, the perfectly spherical combustion chamber with full optical access of ICARE laboratory. This advanced experimental setup allows us to accurately determine the flame speed over a large domain of conditions, scarcely explored, and to generate comprehensive flame speed maps through empirical correlations. A kinetic mechanism was also proposed in this work and was tested on the flame speed data obtained. This mechanism showed more accurate simulations than other performant models available in the literature.

Sensitivity analyses were performed using the present mechanism for both fuels under lean and rich conditions, at different pressures and their corresponding temperatures. These analyses revealed that, relative to equivalence ratio, pressure and temperature have a smaller impact on global reactivity and highlighted the importance of syngas and methane chemistry in controlling the laminar flame speed of methanol and ethanol. Some reactions specific to the former fuel show a notable effect on its flame speed, while those of the latter have a negligible effect compared with the small-molecule reactions.

Finally, further validations were achieved with our mechanism, which shows good predictions for experimental data previously reported (including ignition delay times and JSR data). Therefore, this mechanism proves its ability to serve as a robust core for future kinetic models.

CRediT authorship contribution statement

Bakr Hoblos: Writing – original draft, Visualization, Methodology. **Guillaume Dayma:** Writing – review & editing, Methodology, Conceptualization. **Fabien Halter:** Writing – review & editing, Validation, Methodology, Investigation, Conceptualization. **Zeynep Serinyel:** Writing – review & editing, Methodology, Funding acquisition, Conceptualization.

Declaration of competing interest

The authors declare that they have no known competing financial interests or personal relationships that could have appeared to influence the work reported in this paper.

Acknowledgements

BH thanks the French Ministry of Higher Education and Research (MESR) for a PhD grant. Authors gratefully acknowledge the support received from LabEx CAPRYSSES (ANR-11-LABX-0006-01) and KINOXET (ANR-20-CE05-0017) projects. We also thank Guillaume Jacquet for his valuable contribution.

Appendix A. Supplementary data

Supplementary data to this article can be found online at https://doi.org/10.1016/j.fuel.2026.138358.

Data availability

Data made available as supplementary material

References

[1] Xiouris C, Ye T, Jayachandran J, Egolfopoulos FN. Laminar flame speeds under engine-relevant conditions: uncertainty quantification and minimization in spherically expanding flame experiments. Combust Flame 2016;163:270–83.
[2] Lewis B, von Elbe G. The Recording of pressure and Time in Gas Explosions1. J Am Chem Soc 1933;55:504–7.
[3] Konnov AA, Mohammad A, Kishore VR, Kim NI, Prathap C, Kumar S. A comprehensive review of measurements and data analysis of laminar burning

velocities for various fuel+air mixtures. Prog Energy Combust Sci 2018;68:197–267.
[4] Gülder ÖL. Laminar burning velocities of methanol, ethanol and isooctane-air mixtures. Symp (Int) Combust 1982;19:275–81.
[5] Veloo PS, Wang YL, Egolfopoulos FN, Westbrook CK. A comparative experimental and computational study of methanol, ethanol, and *n*-butanol flames. Combust Flame 2010;157:1989–2004.
[6] Beeckmann J, Cai L, Pitsch H. Experimental investigation of the laminar burning velocities of methanol, ethanol, n-propanol, and n-butanol at high pressure. Fuel 2014;117:340–50.
[7] Raida MB, Hoetmer GJ, Konnov AA, van Oijen JA, de Goey LPH. Laminar burning velocity measurements of ethanol+air and methanol+air flames at atmospheric and elevated pressures using a new Heat Flux setup. Combust Flame 2021;230:111435.
[8] Zheng L, Figueroa-Labastida M, Streicher J, Hanson RK. Measurements and a new correlation of methanol laminar flame speeds at temperatures up to 916 K and elevated pressures behind reflected shock waves. Proc Combust Inst 2024;40:105192.
[9] Zheng L, Figueroa-Labastida M, Nygaard Z, Ferris AM, Hanson RK. Laminar flame speed measurements of ethanol, *iso*-octane, and their binary blends at temperatures up to 1020 K behind reflected shock waves. Fuel 2024;356:129495.
[10] Halter F, Chen Z, Dayma G, Bariki C, Wang Y, Dagaut P, et al. Development of an optically accessible apparatus to characterize the evolution of spherically expanding flames under constant volume conditions. Combust Flame 2020;212:165–76.
[11] Halter F, Dayma G, Serinyel Z, Dagaut P, Chauveau C. Laminar flame speed determination at high pressure and temperature conditions for kinetic schemes assessment. Proc Combust Inst 2021;38:2449–57.
[12] Mouze-Mornettas A, Keck H, Wang Y, Chen Z, Dayma G, Chauveau C, et al. Effect of wall heat transfer on the dynamics of premixed spherical expanding flames. Therm Sci Eng Prog 2022;29:101227.
[13] ANSYS Chemkin 2024 R2, ANSYS Reaction Design: San Diego, 2024.
[14] Serinyel Z, Dayma G, Dagaut P. A detailed high-pressure oxidation study of n-pentanal. Proc Combust Inst 2024;40:105254.
[15] Burke U, Metcalfe WK, Burke SM, Heufer KA, Dagaut P, Curran HJ. A detailed chemical kinetic modeling, ignition delay time and jet-stirred reactor study of methanol oxidation. Combust Flame 2016;165:125–36.
[16] Wang Z, Zhao H, Yan C, Lin Y, Lele AD, Xu W, et al. Methanol oxidation up to 100 atm in a supercritical pressure jet-stirred reactor. Proc Combust Inst 2023;39:445–53.
[17] Mittal G, Burke SM, Davies VA, Parajuli B, Metcalfe WK, Curran HJ. Autoignition of ethanol in a rapid compression machine. Combust Flame 2014;161:1164–71.
[18] Millán-Merino A, Fernández-Tarrazo E, Sánchez-Sanz M, Williams FA. A multipurpose reduced mechanism for ethanol combustion. Combust Flame 2018;193:112–22.
[19] Bagheri G, Ranzi E, Pelucchi M, Parente A, Frassoldati A, Faravelli T. Comprehensive kinetic study of combustion technologies for low environmental impact: MILD and OXY-fuel combustion of methane. Combust Flame 2020;212:142–55.
[20] Zhou C-W, Li Y, Burke U, Banyon C, Somers KP, Ding S, et al. An experimental and chemical kinetic modeling study of 1,3-butadiene combustion: Ignition delay time and laminar flame speed measurements. Combust Flame 2018;197:423–38.
[21] Mouze-Mornettas A, Benito MM, Dayma G, Chauveau C, Cuenot B, Halter F. Laminar flame speed evaluation for CH4/O2 mixtures at high pressure and temperature for rocket engine applications. Proc Combust Inst 2023;39:1833–40.
[22] Leplat N, Dagaut P, Togbé C, Vandooren J. Numerical and experimental study of ethanol combustion and oxidation in laminar premixed flames and in jet-stirred reactor. Combust Flame 2011;158:705–25.
[23] Mathieu O, Pinzón LT, Atherley TM, Mulvihill CR, Schoel I, Petersen EL. Experimental study of ethanol oxidation behind reflected shock waves: Ignition delay time and H2O laser-absorption measurements. Combust Flame 2019;208.